†ELECTRONIC SUPPLEMENTARY INFORMATION for:
Bulk and film synthesis pathways to ternary magnesium tungsten nitrides

Christopher L. Rom,[a,b] Rebecca W. Smaha,[a] Callan A. Knebel,[b] Karen N. Heinselman,[a] James R. Neilson,[b,c] Sage R. Bauers,[a] and Andriy Zakutayev*[a]

[a] *Materials Science Center, National Renewable Energy Laboratory, Golden, CO 80401, USA; E-mail: Andriy.Zakutayev@nrel.gov*
[b] *Department of Chemistry, Colorado State University, Fort Collins, CO, 80523, USA*
[c] *School of Advanced Materials Discovery, Colorado State University, Fort Collins, CO, 80523, USA*

Contents

Additional experimental details

This manuscript combines synthetic techniques from multiple disciplines. As readers may not have personal experience with all three synthesis techniques, we diagram them in Figure S1. For additional information on the synthesis (and characterization) capabilities at NREL, we direct the reader to the following webpage: https://www.nrel.gov/materials-science/materials-synthesis-characterization.html

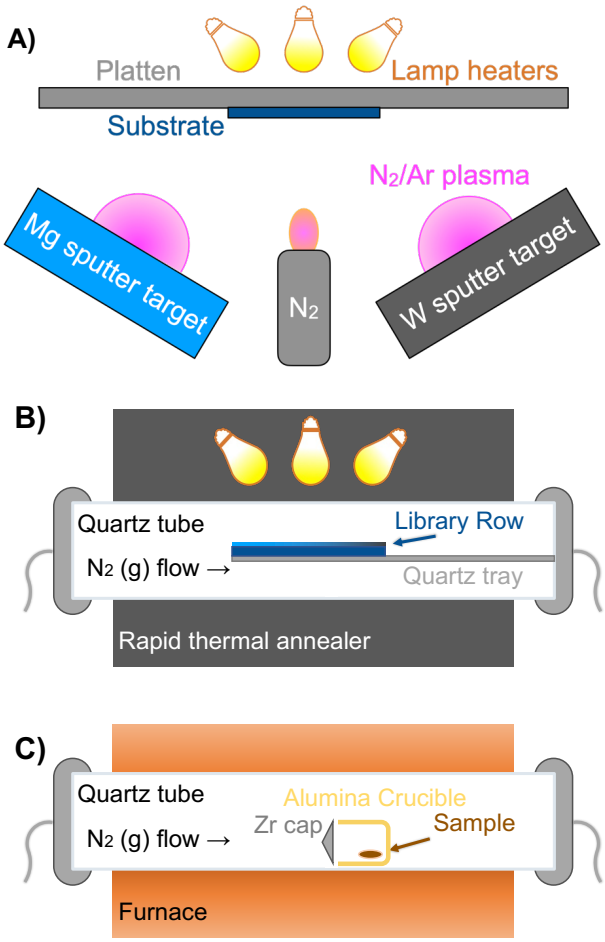

Figure S1 Three experimental setups used for the synthesis of Mg-W-N phases: A) combinatorial sputtering, B) rapid thermal annealing of combinatorial libraries, and C) bulk solid state syntheses.

Mg-poor phases

Mg-poor phases show slightly different structures between annealed films and films deposited at elevated substrate temperatures (Figure S2). The $Fm\bar{3}m$ structure that best matches the Mg-poor phases from our combinatorial depositions at elevated temperatures. Therefore, we classify these compounds as the RS structure. However, the Mg-poor samples deposited at ambient conditions and subsequently annealed under flowing nitrogen are not well fit by the $Fm\bar{3}m$ structure. The 2θ spacing between the two observed reflections is too large to match the expected the $Fm\bar{3}m$ reflections of (111) and (200) planes. Given the complexity of the W-N binary system and the sparcity of observed reflections, we refer to the Mg-poor phases in annealed libraries as WN_x rather than the RS structure. This difference may stem from the elevated nitrogen chemical potential present in combinatorial depositions but absent during annealing.

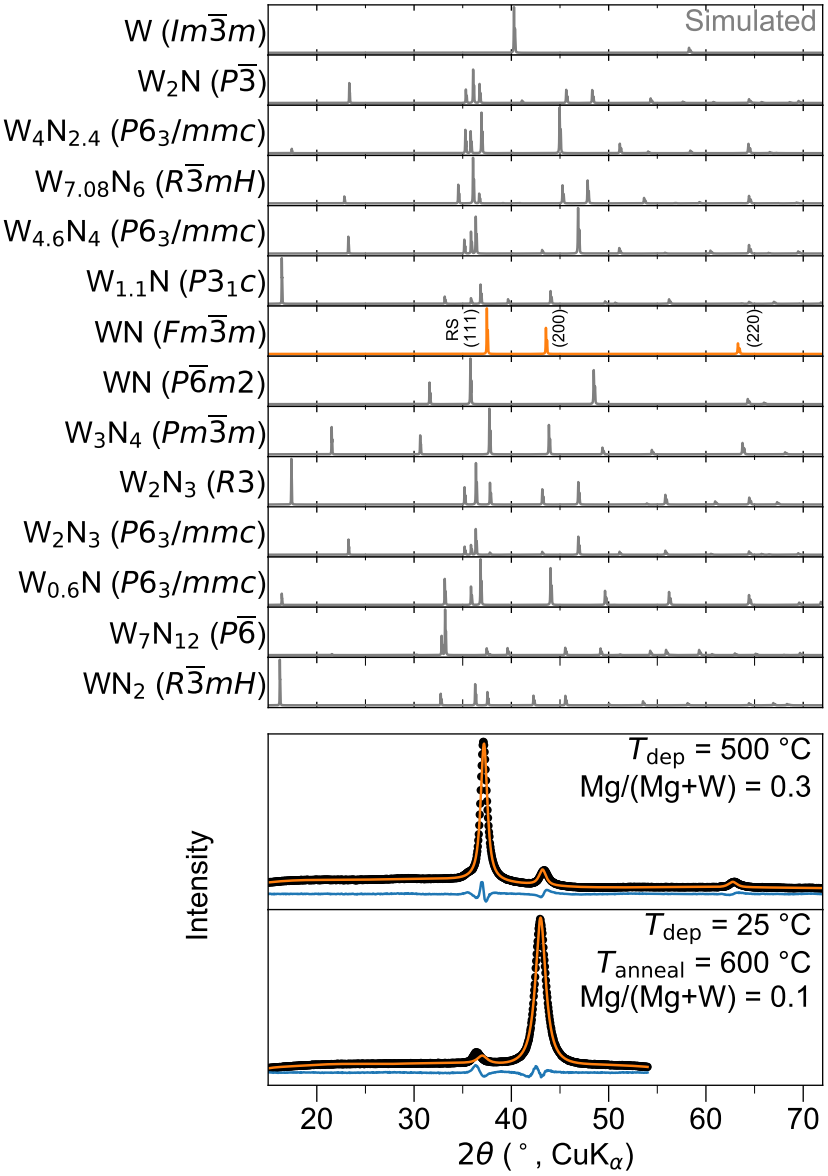

Figure S2 LeBail refinements of laboratory XRD data using the $Fm\bar{3}m$ structure for a sample deposited at 500 °C compared with a sample deposited at ambient conditions and annealed at 500 °C. Simulated patterns for WN_x phases are shown for reference.

Crystallographic details

Rietveld analysis suggests some cation site disorder may exist in RL $MgWN_2$ (Table S1). Refinements were performed in TOPAS v6 with the inversion parameter x constrained to ensure full occupancy at both cation sites; $(Mg_{1-x}W_x)(W_{1-x}Mg_x)N_2$.

Table S1 Refined atomic coordinates for RL $MgWN_2$ in space group $P6_3/mmc$ from laboratory PXRD (Cu K_α). Unit cell parameters were $a = 2.91097(4)$ Å and $c = 10.5857(2)$ Å. Lorentzian size broadening refined to 126(2) nm crystallite domain length. $R_{exp} = 8.40437071$, $R_{wp} = 10.3085532$, G.o.F. = 1.2265705

Wyckoff site	Atom	Multiplicity	x	y	z	Occ.	$B(^2)$
2a	Mg	2	0	0	0	0.885(10)	0.1(6)
2a	W	2	0	0	0	0.115(10)	0.1(6)
2d	W	6	1/3	2/3	0.75	0.885(10)	3.39(7)
2d	Mg	6	1/3	2/3	0.75	0.115(10)	3.39(7)
4f	N	12	1/3	2/3	0.1453(14)	1	7.4(5)

As thin film samples exhibited texturing (i.e., preferred orientation), Rietveld analysis was not appropriate for determining atomic occupancy. Instead, Lebail fits were performed on GIWAXS data to estimate lattice parameters (Table S2). The lattice parameters for thin films of RS $MgWN_2$ (4.29 Å) and Mg_3WN_4 (4.30 Å) are similar to those reported by Bauers et al. for RS $MgTiN_2$ (4.26 Å), $MgZrN_2$ (4.54 Å), $MgHfN_2$ (4.52 Å), and Mg_2NbN_3 (4.37 Å).[1] The lattice parameters for the thin film RL phase are slightly smaller than those refined for the bulk RL phase (Table S1), possibly owing to sample misalignment for the thin film measurement. The h-BN Mg_3WN_4 does not have a readily comparable structure, but the refined unit cell parameters lead to reasonable bond lengths given the atomic positions (M x = 1/3, y = 2/3, z = 1/4; N x = 1/3, y = 2/3, z = 3/4). The axial M-N bond is 2.24 Å and the equatorial M-N bond is 2.04 Å, which is similar to the 2.15 Å M-N bond for RS Mg_3WN_4. The typical grain size of sputtered ternary metal nitride thin films is 30-50 nm and the typical surface roughness is < 5 nm, but we cannot reliably report the refined crystallite size for these samples as the sample geometry also contributed to peak broadening.

Table S2 Lattice parameters extracted from Lebail refinements of GIWAXS data.

Composition	Condition	Polymorph	a (Å)	c (Å)
$MgWN_2$	$T_{anneal} = 600$ °C	RS	4.29	-
$MgWN_2$	$T_{anneal} = 900$ °C	RL	2.89	10.54
Mg_3WN_4	$T_{anneal} = 600$ °C	RS	4.30	-
Mg_3WN_4	$T_{anneal} = 900$ °C	RS	4.30	-
Mg_3WN_4	$T_{dep} = 25$ °C	h-BN	3.53	4.47

Annealing experiments

RTA experiments conducted on an as-grown sample of h-BN Mg_3WN_4 reveal that heating this polymorph drives a conversion to the RS polymorph starting near T_{anneal}=700 °C for 3 min, with complete conversion occurring by 900 °C (Figure S3). These films were capped with approximately 20 nm of TiN to prevent Mg loss by volatization during annealing. This TiN layer is too thin to be detected in these XRD measurements. This result suggests that h-BN structure of Mg_3WN_4 may be metastable with respect to the RS polymorph. In contrast, annealing the RS polymorph of Mg_3WN_4 does not drive any additional structural changes that are detectable by diffraction (Figure S4).

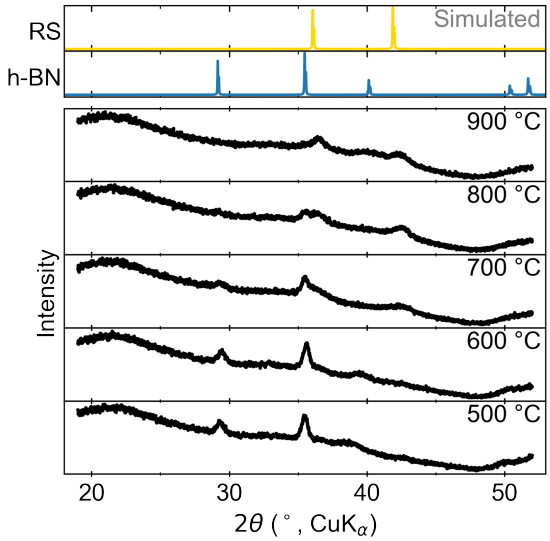

Figure S3 Rapid thermal annealing experiments show that the h-BN structure converts to the RS structure as T_{anneal} increases, suggesting the h-BN structure is metastable relative to the RS structure. These films were capped with a 20 nm layer of TiN to minimize Mg loss by volatility.

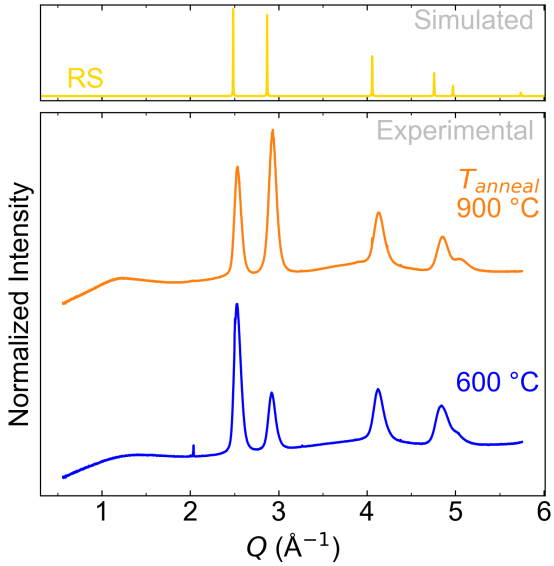

Figure S4 GIWAXS patterns for a sample of Mg_3WN_4 annealed at 600 ℃ and 900 ℃ show that the initial RS structure persists through these anneals. Differences in peak intensity stem from initial texturing of the deposited film, rather than changes due to annealing.

Simulating cation disorder

Simulated PXRD patterns provide insight on the expected diffraction patterns for differing degrees of cation ordering. The $P6_3/mmc$ structure of the RL $MgWN_2$ phase is primarily defined by alternating layers of Mg octahedra and W trigonal prisms (Figure 1B). However, those coordination environments could persist with varying degrees of cation disorder across those two metal sites. Figure S5 shows how cation disorder decreases the intensity of the (002) reflection relative to other peaks.

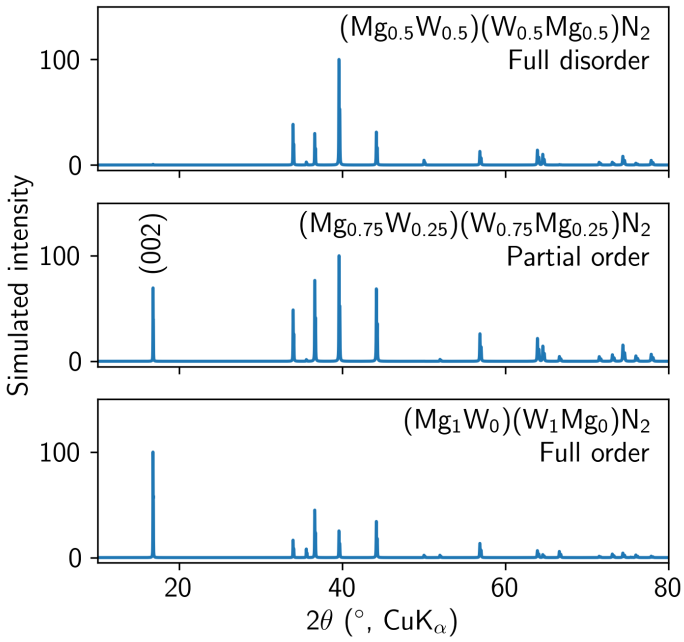

Figure S5 Simulated diffraction patterns for the $MgWN_2$ phase in the RL polymorph ($P6_3/mmc$) with full cation disorder (top), partial cation disorder (middle), and full cation order (bottom). The relative intensity of the (002) reflection increases with increasing ordering. Patterns were simulated with VESTA software.[2]

RBS measurements

Rutherford backscattering (RBS) measurements were conducted to assess N and O ratios. Select samples were deposited on a glassy carbon substrate to better resolve N and O profiles in RBS. N and O content extracted from the fits appears greater than the expected cation:anion ratio of 1:1, but we believe RBS overestimates anion content owing to difficulty in fitting such light elements when comingled with heavy W. However, as O and N are similarly affected by any systematic error, O/(N+O) ratios are still comparable sample to sample. O content increases with increasing Mg content (Figure S6), even when a TiN capping layer is applied prior to removing the sample from the deposition chamber. This trend suggests the O may come from the Mg target or the sputtering atmosphere, rather than from reaction with air after deposition.

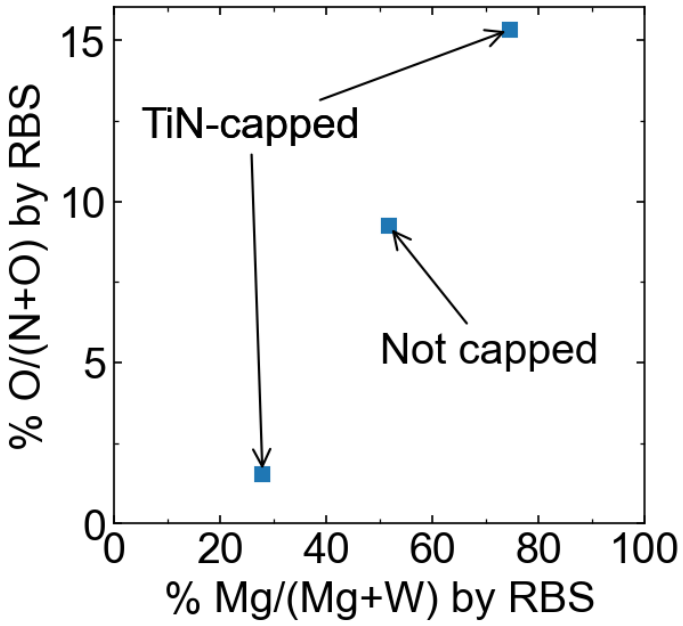

Figure S6 Oxygen as a percentage of total anions increases with increasing Mg content. Spectra are shown in Figure S7.

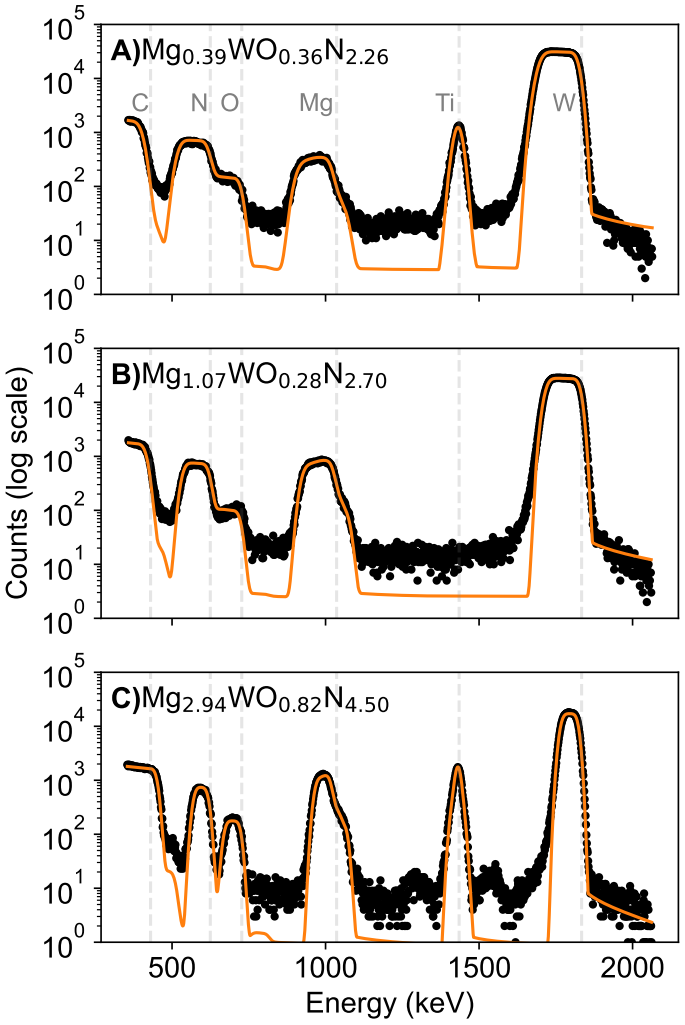

Figure S7 RBS spectra and fits of Mg-W-N films on a carbon substrate with A) Mg-poor RS, B) nominally $MgWN_2$ RS and C) nominally Mg_3WN_4 h-BN. The films in A) and C) were capped with TiN to prevent air exposure. Compositions were normalized to the W signal.

AES measurements

Depth profiling by Auger electron spectroscopy (AES) was conducted on select films annealed at 600 °C and 900 °C (Figure S8). These measurements show a surface oxide layer consistent with MgO, and low oxygen levels throughout the remaining depth of the films. These oxygen levels contrast with those detected by RBS on h-BN Mg_3WN_4 suggesting oxide content may play a role in relative stability of the RS and h-BN structures. However, RS Mg_3WN_4 is also present in the same libraries as h-BN Mg_3WN_4 (sometimes even co-occurring in the same sample, Figure 2), suggesting similar oxygen content for both RS and h-BN Mg_3WN_4. As systematically varying and measuring O/(N+O) is beyond the scope of this study, we cannot make definitive statements on the influence of oxygen on these structures.

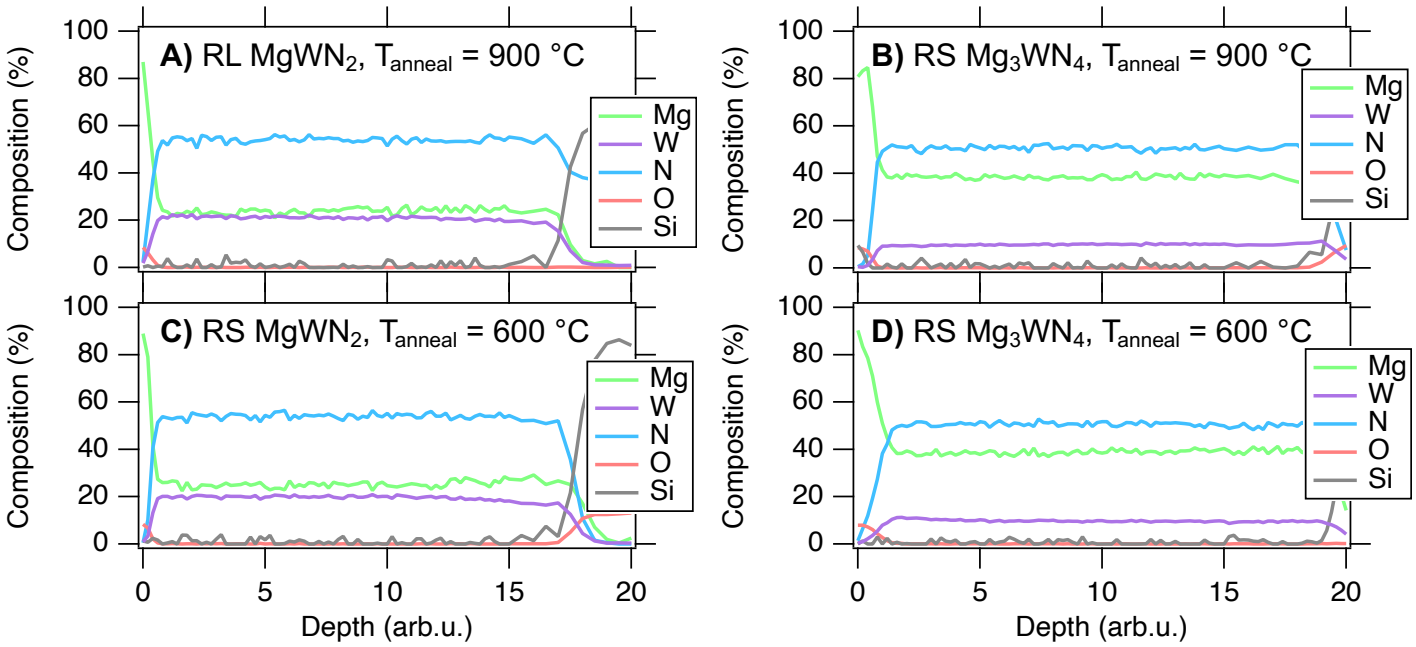

Figure S8 AES depth profiles of $MgWN_2$ (A and C) and Mg_3WN_4 (B and D) films annealed at T_{anneal} = 900 ℃ (A and B) or 600 ℃ (C and D). Composition values were calibrated to the Mg/(Mg+W) ratio for $MgWN_2$ (T_{anneal} = 900 ℃) determined by XRF.

Electronic structure calculations

Non-self-consistent field (NSCF) calculations on a uniform k-point mesh reveal a 1.18 eV indirect bandgap for RL $MgWN_2$ (Figures 5 and S9). The valance and conduction bands are both comprised primarily of W d and N p states, indicating covalency in the W-N bonds. The bandgap is consistent with $d-d$ transitions expected for the $5d^2$ electron configuration of W^{4+} in trigonal prismatic environment (Figure 5B).[3–5] In contrast, the RS polymorph of $MgWN_2$ exhibits a metallic band structure (Figure S10), owing to the octahedral environment for W^{4+} (Figure 5D).

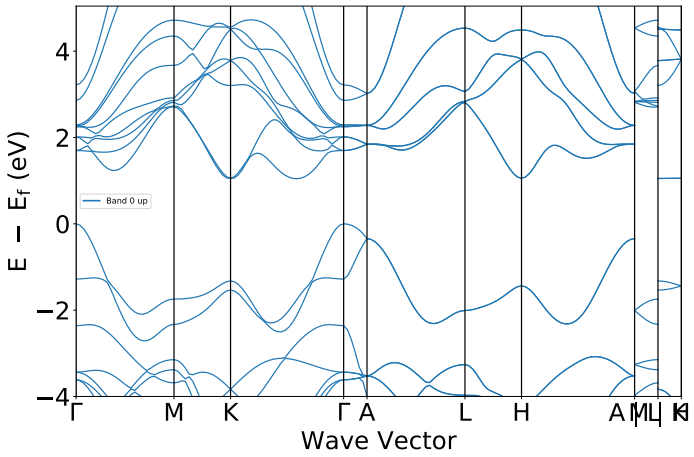

Figure S9 Calculated band structure for cation-ordered RL $MgWN_2$ (space group $P6_3/mmc$).

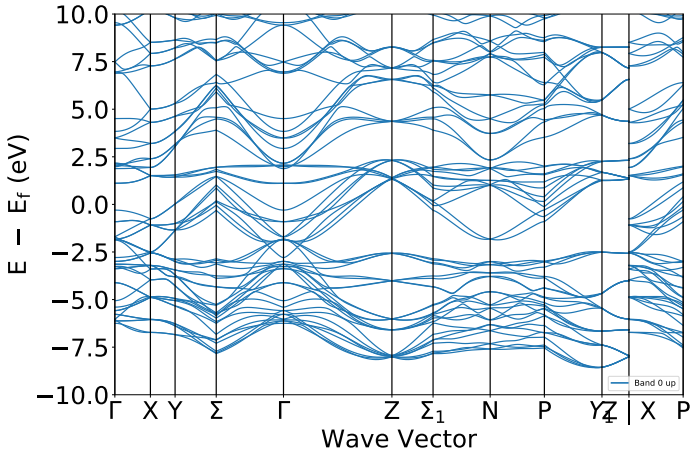

Figure S10 Calculated band structure for cation-ordered RS $MgWN_2$ (space group $I4_1/amd$).

Electronic property measurements

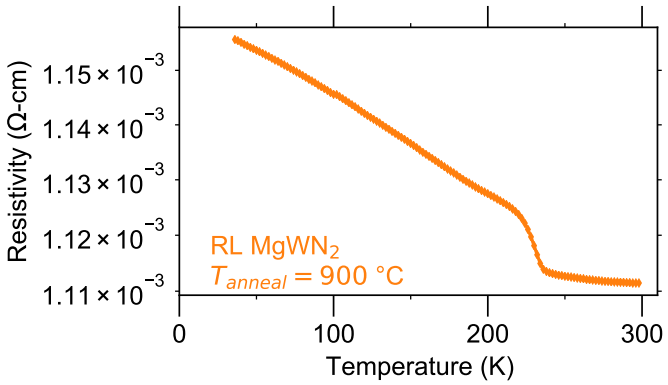

Figure S11 Temperature dependent resistivity measurements of RL $MgWN_2$ ($T_{anneal} = 900$ ℃) from Figure 6A, replotted on a narrower vertical axis to show the small decrease in resistivity with increasing temperature. The inflection near 230 K is an artefact of the instrument.[6–9]

Notes and references

[1] S. R. Bauers, A. Holder, W. Sun, C. L. Melamed, R. Woods-Robinson, J. Mangum, J. Perkins, W. Tumas, B. Gorman, A. Tamboli et al., Proceedings of the National Academy of Sciences, 2019, **116**, 14829–14834.

[2] K. Momma and F. Izumi, Journal of applied crystallography, 2011, **44**, 1272–1276.

[3] R. Kasowski, Physical Review Letters, 1973, **30**, 1175.

[4] L. Mattheiss, Physical Review Letters, 1973, **30**, 784.

[5] R. Verrelli, M. E. Arroyo-de Dompablo, D. Tchitchekova, A. Black, C. Frontera, A. Fuertes and M. R. Palacin, Physical Chemistry Chemical Physics, 2017, **19**, 26435–26441.

[6] R. W. Smaha, J. S. Mangum, I. A. Leahy, J. Calder, M. P. Hautzinger, C. P. Muzzillo, C. L. Perkins, K. R. Talley, S. Eley, P. Gorai et al., arXiv preprint arXiv:2305.00098, 2023.

[7] S. R. Bauers, D. M. Hamann, A. Patterson, J. D. Perkins, K. R. Talley and A. Zakutayev, Japanese Journal of Applied Physics, 2019, **58**, SC1015.

[8] S. R. Bauers, J. Mangum, S. P. Harvey, J. D. Perkins, B. Gorman and A. Zakutayev, Applied Physics Letters, 2020, **116**, 102102.

[9] C. L. Rom, R. W. Smaha, C. L. Melamed, R. R. Schnepf, K. N. Heinselman, J. S. Mangum, S.-J. Lee, S. Lany, L. T. Schelhas, A. L. Greenaway et al., Chemistry of Materials, 2023, **35**, 2936–2946.